ACS OMEGA

http://pubs.acs.org/journal/acsodf

Article

Experimental and Numerical Investigation into the Heat- and Mass-Transfer Processes of *n*-Butane Adsorption on Activated Carbon

Fei Zhao, Ling Zhu,* Zhenzhong Wang, Yan Hou, Jiaqing Chen, Chunyu Wang, and Danyun Xu

Cite This: *ACS Omega* 2021, 6, 17162−17172

Read Online

ACCESS | Metrics & More | Article Recommendations

ABSTRACT: In this work, the adsorption parameters of *n*-butane vapor on an absorbent were tested following the fixed-bed method. According to the corresponding experiments, the maximum adsorption capacity and breakthrough time of activated carbon (AC) are 0.2674 $g \cdot g^{-1}$ and 924 min, respectively. According to the two-energy-state model formula and the classical adsorption heat formula, the values of theoretical and actual adsorption heat of AC adsorbing *n*-butane are 5.48 and 5.56 $kJ \cdot mol^{-1}$, respectively. The model for adsorption of *n*-butane by an AC fixed bed is based on the analytical solutions to the mass, momentum, and energy conservation equations. The model is built using porous media zone in ANSYS Fluent, the implementation of the model into ANSYS Fluent under user-defined functions (UDFs) is also described, the mass source term S_i and energy source term S_T are loaded into Fluent through UDF, and then the mass- and heat-transfer processes of AC in the absorption of *n*-butane are simulated. Furthermore, the predictions by ANSYS Fluent are compared with in situ experimental data, and the deviation rate of breakthrough time and temperature of six monitoring points is less than 5%. The results verify the accuracy and feasibility of computational fluid dynamics (CFD). Therefore, the model can be used to predict the engineering application of the adsorption of organic gases by various porous media.

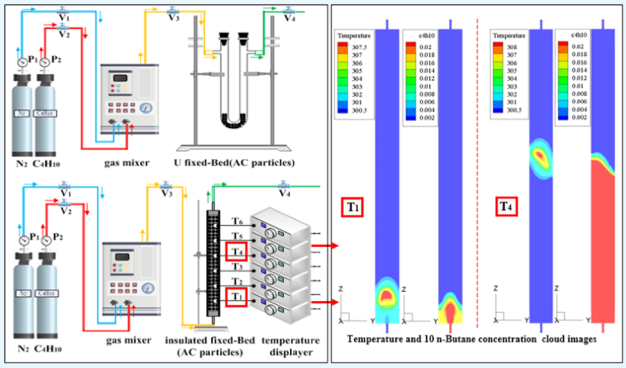

1. INTRODUCTION

According to the World Health Organization (WHO), volatile organic compounds (VOCs) are organic compounds with a Reid vapor pressure exceeding 10.3 Pa at the normal temperature (293.15 K) and pressure (101.325 kPa).[1] VOCs are a large group of carbon-based chemicals that easily evaporate at room temperature, including alkanes, aromatics, esters, alkenes, carboxylic acids, and alcohols.[2−7] VOCs are classified as major contributors to air pollution owing to their persistence and tendency to accumulate in the environment.[8,9]

They contribute to pollution both indirectly and directly as ozone/smog precursors and substances toxic to the environment, respectively.[10,11]

Activated carbon (AC) is one of the most effective absorbents for VOCs owing to its specific surface area, pore-size distribution,[8,12−16] and the chemical affinity between the adsorbents and VOC pollutants. To further improve the adsorption efficiency, deep investigations into modified AC materials have received more attention, with modification processes including the rebuilding of pore structures to match the pore size of adsorbents to the molecular diameter of gaseous VOCs. Transport phenomena, such as heat and mass transfer in porous AC, have an important effect on the adsorption processes and their efficiency. An absorbent with a higher adsorption heat and lower heat-transfer efficiency would cause an increase in the temperature of the adsorbent bed, which is the major factor causing the adsorption performance to degrade and affecting the regeneration efficiency. Moreover, when the adsorbent bed temperature exceeds the flashing point of VOCs, some serious accidents would occur, such as fire or an explosion in the adsorption device. A computational fluid dynamics (CFD) approach is used for modeling transport and adsorption in porous media using Fluent. Much work has already been conducted in this area.[17−20]

For example, Bahadori et al. investigated the effect of variations in viscosity on natural convection in a saturated enclosure, predicting the flow field and heat transfer in double-layer porous media using the Darcy model in a CFD commercial package, but did not simulate or analyze the concentration field.[21] Hou et al. established the computational domain model of the onboard refueling vapor recovery (ORVR) carbon canister and simulated the internal structure of carbon using a

Received: December 25, 2020
Accepted: May 28, 2021
Published: June 25, 2021

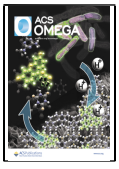

https://doi.org/10.1021/acsomega.0c06273
ACS Omega 2021, 6, 17162−17172

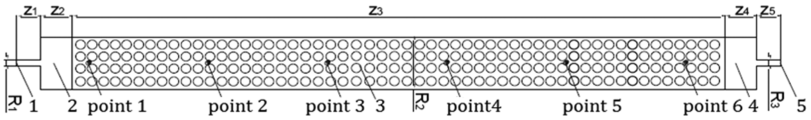

Figure 1. Geometric sketch of the fixed bed.

porous medium model. The internal pressure fields of the carbon canister's adsorption and desorption processes were also numerically simulated by Fluent,[22] while the temperature and concentration were not considered. Bai et al. simulated fixed-bed adiabatic adsorption/desorption processes and used the linear driving force model for the heat- and mass-transfer rates. They also used a two-dimensional cylindrical canister and three-dimensional automotive production canister geometry to study the adsorption/desorption processes of carbon dioxide in a helium carrier gas on Norit B4 AC.[23] However, their simulation results differed from the experimental results. Lin et al. presented a test process based on the analytical simulation of the butane working capacity (BWC) of an automotive carbon canister and based their computational model of the fixed-bed system of a carbon canister on nonequilibrium, nonisothermal, and non-adiabatic algorithms to simulate the real-life loading/purging of hydrocarbon vapors from this device.[24] However, the thermal transportation and temperature fields were not considered in their studies. Hou established the unsteady three-dimensional mathematical model for the absorption of benzene by AC absorption, and the effects of the inlet benzene concentration and gas velocity on outlet benzene concentration, temperature, and pressure distribution in the U-tube were investigated.[25,26] The fixed bed was considered an integral solid, so the effects of bed porosity and transfer resistance were not investigated.

In this paper, adsorption experiments, theoretical calculations of adsorption heat, and numerical simulations were used. The objective of this work is to investigate the mass- and heat-transfer properties during the adsorption of *n*-butane on AC in the fixed bed. The adsorption experiment was carried out on the fixed bed with a frequently used AC. The temperature of the fixed bed and the concentration of *n*-butane at the outlet were measured. Several kinetic models were used to fit and analyze the adsorption breakthrough curve, which was measured in the adsorption experiment. According to the formula of adsorption heat, the theoretical adsorption heat and the actual adsorption heat of *n*-butane adsorbed on AC were calculated. Based on the experimental data, the expressions of mass source term (S_i) and energy source term (S_T) for the simulation model were obtained. The fixed-bed model was implemented following a finite volume method in the commercial CFD package Fluent, the same initial conditions as the adsorption experiment were setup in Fluent. The mass- and heat-transfer processes of AC adsorbing *n*-butane were simulated by loading the S_i and S_T with user-defined functions (UDFs). Validations of the newly introduced model predictions are demonstrated through comparisons with experimental results.

2. RESULTS AND DISCUSSION

To understand the heat and mass transfer during adsorption on the fixed bed, a mathematical model of the adsorption of *n*-butane on an AC fixed bed was established based on mass, energy, and momentum equations. The Integrated Computer Engineering and Manufacturing (ICEM) code was used to establish the physical model and generate the grid, and Fluent was used for simulations. Adsorption was modeled as a flow through a porous medium, with the mass and energy source terms defined in the UDF. The binary gas mixture flow in the porous zone with the laminar fluid flow was simulated using the built-in solver. The results obtained were quantitatively analyzed with a three-dimensional numerical model that solves the nonstationary continuity, momentum, and energy equations, which allows the spatial distributions of the temperature and adsorbed quantities to be simulated.

2.1. Physical Model. The geometric diagram of the fixed bed presented in Figure 1 consists of five parts. The inlet size was $R_1 = 2$ mm, $z_1 = 15$ mm; the cavity radius was $R_2 = 17.5$ mm, and the total length was 480 mm. The front buffer length was $z_2 = 20$ mm, the AC particle area length was $z_3 = 410$ mm, and the tail buffer length was $z_4 = 20$ mm; the outlet (R_3, z_5) was of the same size as the inlet. There were six temperature measuring points in the vertical direction on the side of the fixed bed with a straight tube, which were marked as points 1−6, respectively.

The size of the physical model was set according to the actual size of the fixed bed. The structured and unstructured grids were combined to divide the mesh. The number of meshes was 12 871. The mesh of the geometric body was divided, as shown in Figure 2.

Figure 2. Fixed-bed model mesh-generation diagram.

2.2. Mathematical Model. The adsorption of *n*-butane by AC is a three-dimensional, unsteady process that follows the mass, momentum, and energy conservation laws. Fluent was used to simulate the adsorption process, and the mathematical models for numerical simulations were based on the mass, momentum, and energy conservation equations. A complete mathematical model with mass, momentum, and energy equations was established.

2.2.1. Mass Conservation Equation. The mass conservation equation (eq 1)[27−31] can be expressed as

$$\frac{\partial \varepsilon \rho_f}{\partial t} + \nabla(\varepsilon \rho_f \cdot u) = -S_m, \quad \left(S_m = \sum_{i=1}^{n} S_i\right) \tag{1}$$

where ρ_f is the fluid density (kg·m^{-3}), t is the time (s), ε is the porosity of AC, u is the fluid local velocity (m·s^{-1}), and S_m is the generalized mass source term (kg·m^{-3}·s^{-1}), and S_i is the mass source term of gas i (kg·m^{-3}·s^{-1}).

The adsorbed phase mass conservation eqs 2 and 3[27,32] can be expressed as

$$\frac{\partial}{\partial t}(\varepsilon \rho_f Y_i) + \nabla\cdot(\varepsilon \rho_f u Y_i) - \nabla\cdot(\varepsilon \rho_f D_{i,m} \nabla Y_i) = -S_i \tag{2}$$

$$S_i = (1 - \varepsilon)\rho_{AC} M_i \frac{\partial q_i}{\partial t} \tag{3}$$

where Y_i is the mass fraction of gas i, D_i is the diffusion coefficient of gas i, M_i is the amount of the substance of gas i (kg·m^{-3}), q_i is

https://doi.org/10.1021/acsomega.0c06273
ACS Omega 2021, 6, 17162−17172

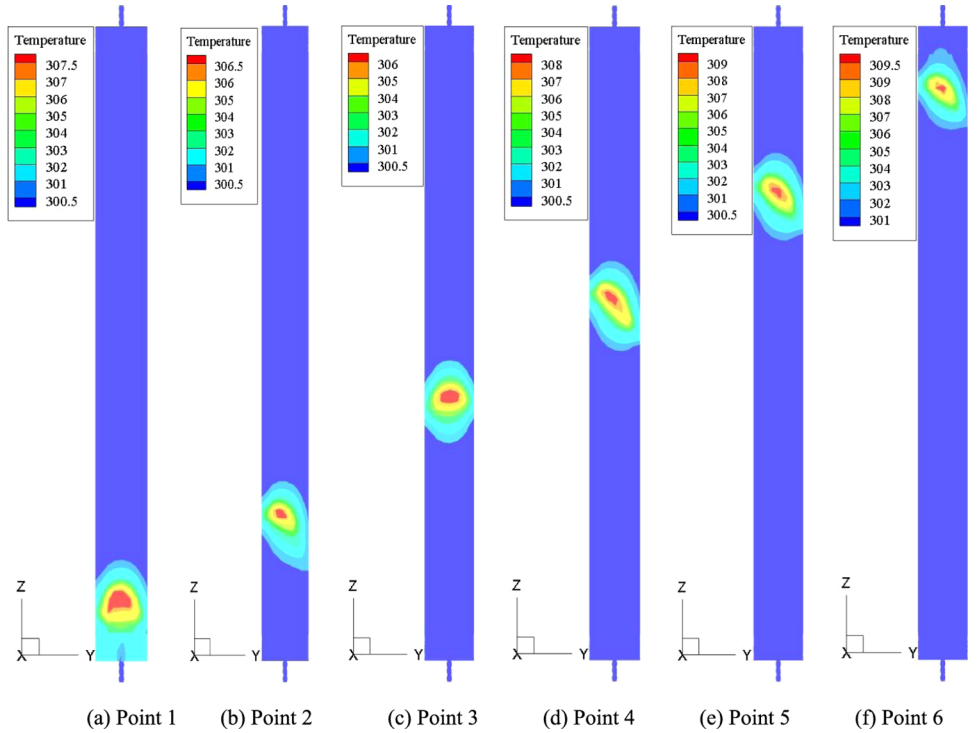

Figure 3. Temperature cloud images of the adsorption process.

the gas concentration ($kg \cdot m^{-3}$), and ρ_{AC} is the density of AC ($kg \cdot m^{-3}$).

2.2.2. Momentum Conservation Equation. The momentum conservation equation (eq 4)[27,30−32] can be expressed as

$$\frac{\partial}{\partial t}\rho_f u_i + \nabla \cdot \rho_f u u_i = -\nabla p + \mu \nabla^2 u + \frac{\mu}{3}\nabla\nabla \cdot u + \rho_f g + S_V \tag{4}$$

where u_i is the velocity of gas i ($m \cdot s^{-1}$), μ is the viscosity (Pa·s), and S_V is the momentum source term ($N \cdot m^{-3}$).

The porous medium model is a momentum source term superimposed on the momentum equation. The source term includes two parts, i.e., the viscous and inertial loss terms, as shown in eq 5[37,40]

$$S_V = -\left(\frac{\mu}{\alpha} v_i + C_2 \frac{1}{2}\rho_f |v_m| v_i\right) \tag{5}$$

where α is the Darcy permeability coefficient (m^2), C_2 is the inertial resistance (m^{-1}), ν_m is the velocity ($m \cdot s^{-1}$), and ν_i is the velocity for i (x, y, or z) ($m \cdot s^{-1}$).

There are two resistance coefficients in the porous simulation process, i.e., viscous resistance $1/\alpha$ and inertial resistance C_2, which can be calculated according to Ergun equation (eq 6)[30,33]

$$\frac{1}{\alpha} = \frac{150}{D_p^2}\frac{(1-\varepsilon)^2}{\varepsilon^3} = 5.5267 \times 10^8\ m^{-2}\ C_2$$
$$= \frac{3.5}{D_p}\frac{(1-\varepsilon)}{\varepsilon^3} = 46\,525\ m^{-1} \tag{6}$$

where ε is the porosity of AC (0.38), D_p is the mean particle diameter of AC (0.00085 m), and $1/\alpha$ is the viscous resistance (m^{-2}).

2.2.3. Energy Conservation Equation. The energy conservation equation[27−29] can be expressed as

$$\frac{\partial(\rho_f T)}{\partial t} + \frac{\partial(\rho_f u T)}{\partial x} + \frac{\partial(\rho_f v T)}{\partial y} + \frac{\partial(\rho_f w T)}{\partial z} = \frac{\partial}{\partial x}\left(\frac{k_h}{c_p}\frac{\partial T}{\partial x}\right) + \frac{\partial}{\partial y}\left(\frac{k_h}{c_p}\frac{\partial T}{\partial y}\right) + \frac{\partial}{\partial z}\left(\frac{k_h}{c_p}\frac{\partial T}{\partial z}\right) + S_T \tag{7}$$

where c_p is the specific heat capacity ($J \cdot kg^{-1} \cdot °C^{-1}$), T is the temperature (°C), k_h is the heat-transfer coefficient of the fluid ($W \cdot K \cdot m^{-2}$), and S_T is the generalized energy source term ($W \cdot m^{-3}$). x, y, and z are three directions of the space coordinate system and u, v, and w are the local fluid velocities in the x, y, and z directions ($m \cdot s^{-1}$).

2.2.4. Adsorbed Phase Mass Balance Equation. The adsorbed phase mass balance equation[32,34] for component i can be expressed as

$$\frac{\partial q_i}{\partial t} = k_i(q_i^* - q_i) \tag{8}$$

where k_i is the mass-transfer coefficient and q_i^* is the gas equilibrium concentration.

According to the first-order kinetics fitting equation $q = 51.822 - 51.822\,e^{-0.02386t}$ (Figure 14), it can be calculated that

$$\frac{dq}{dt} = k_1(q_e - q) = 51.822\,e^{-0.02386t}$$

The adsorbed phase mass source term S_i in eq 2 can be expressed as

$$S_i = \frac{dm_{C_4H_{10}}}{dt \cdot dV_{AC}} = \frac{dq \cdot dm_{AC}}{dt \cdot dV_{AC}} = \frac{dq}{dt} \cdot \rho_{AC}$$
$$= \frac{51.822}{10^3} e^{-0.02386t/60} \cdot 550\ kg \cdot m^{-3} = 28.5021 e^{-0.02386t/60}$$
$$kg \cdot m^{-3} \cdot s^{-1}$$

https://doi.org/10.1021/acsomega.0c06273
ACS Omega 2021, 6, 17162−17172

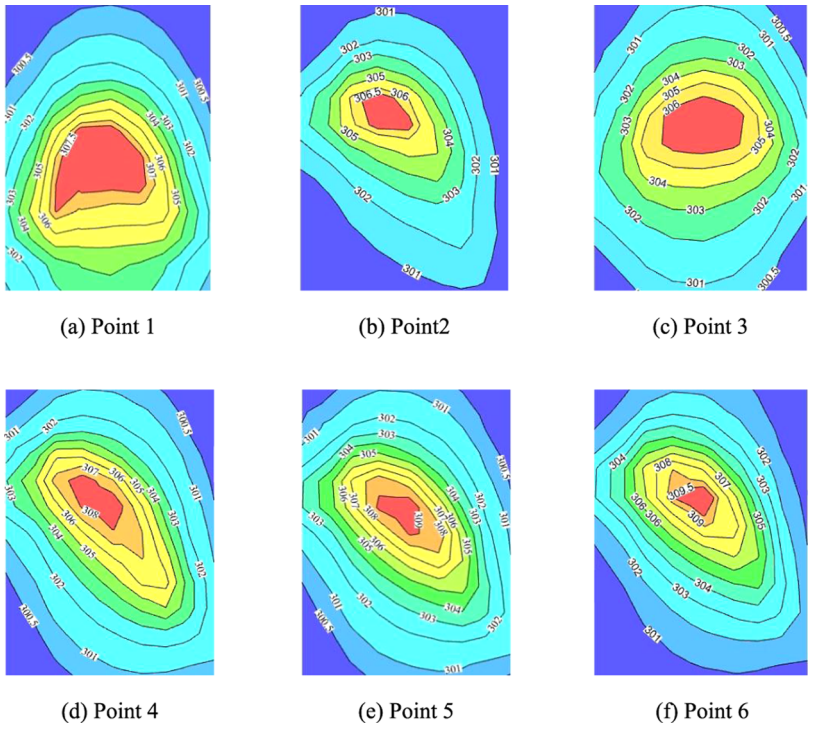

Figure 4. Local temperature isoline plots of the adsorption process.

where $m_{C_4H_{10}}$ is the mass of *n*-butane (g), m_{AC} is the mass of AC (g), V_{AC} is the volume of AC (m^3), and ρ_{AC} is the density of AC (550 kg·m^{-3}).

Adsorption heat of *n*-butane on AC: $Q_{a,a}$ = 5.56 kJ·mol^{-1}, the energy source term S_T in eq 15 can be expressed as

$$S_T = \frac{S_i}{M_{C_4H_{10}}} \cdot Q_{a,a} = \frac{28.5021\ e^{-0.02386t/60}(kg \cdot m^{-3} \cdot s^{-1})}{58.12\ g \cdot mol^{-1}}$$
$$\cdot 5.56\ kJ \cdot mol^{-1} = 2.7266 \times 10^6\ e^{-0.02386t/60}\ W \cdot m^{-3}$$

where $M_{C_4H_{10}}$ is the molar mass of *n*-butane (58.12 g·mol^{-1}).

To generate a simulation result with acceptable accuracy in comparison to the experimental data, it is necessary to select models for the specific situation in Fluent. When Fluent is used for calculation, the N−S equation is set as the governing equation and the calculation type is set to be implicit and pressure-based. The physical model is imported into Fluent, and the species transfer model, laminar flow model, and porous medium model were used. The inlet velocity boundary condition was applied at the left end of the fixed bed, and a pressure outlet boundary condition was applied at the exit. The mass source term S_i and energy source term S_T were loaded into Fluent through UDF, and the model of *n*-butane adsorption on AC fixed bed was established.

2.3. Simulation Results and Discussion. The initial parameters of the model are set according to the experimental conditions. The inlet condition of the model is the velocity inlet, the boundary condition is the wall, and the outlet condition is the outlet vent. The inlet speed was set to 0.5305 m·s^{-1}, the inlet concentration was 0.02 ($V_{C_4H_{10}}$/V), and the initial temperature was 300 K, the viscous resistance of the porous medium area was set to 5.5267×10^8 m^{-2}, and the inertial resistance of the porous medium area was set to 4.6525×10^4 m^{-1}.

It took 895 min to simulate the whole adsorption process using Fluent. After simulations, the temperature and concentration cloud images were obtained using the Tecplot postprocessing software. The adsorption process was analyzed using the experimental data, simulated results, and simulated cloud images.

2.3.1. Cloud Image Analysis. In this study, the cloud images of six points in the fixed bed were selected for analysis.

As is known, during gas-phase adsorption, a high amount of heat is released. The isosteric and limit heat of adsorption of AC are 17.25−21.5 and 22.5 kJ·mol^{-1}, respectively.[35] The heat-transfer coefficient of AC is 0.15−0.20 W·m^{-1}·K^{-1}.[35−37] As this value is low, the heat of adsorption cannot be quickly transferred to the outside environment. The heat of adsorption accumulates internally, resulting in a local temperature increase in the fixed bed. The temperature cloud images of the fixed bed are shown in Figure 3, and the local temperature isoline plots of the adsorption process are shown in Figure 4.

Figure 3 shows that the local heating zone of the fixed bed moves forward along the airflow. The maximum temperature in the high-temperature area of the six monitoring points is 306−309.5 K. As soon as AC adsorbed and saturated, it would no longer release heat. When the mixed gas kept on passing through the adsorption saturation region, it would act as sweeping gas and remove the heat gathered in the fixed bed, resulting in a temperature decrease in the saturated region. For example, Figure 4a shows that the adsorption of *n*-butane occurs in the area of point 1, and the temperature of point 1 reaches the maximum. From Figure 4a,b, we can find that when the AC in the area of point 1 is saturated, the adsorption moves forward to the area of point 2, and the temperature of point 2 increases gradually and reaches the maximum. As the continuous sweeping of the gas transfers the locally increased heat to the fixed bed at the back of the unsaturated part, the temperature of point 1 decreases to the background temperature.

https://doi.org/10.1021/acsomega.0c06273
ACS Omega 2021, 6, 17162−17172

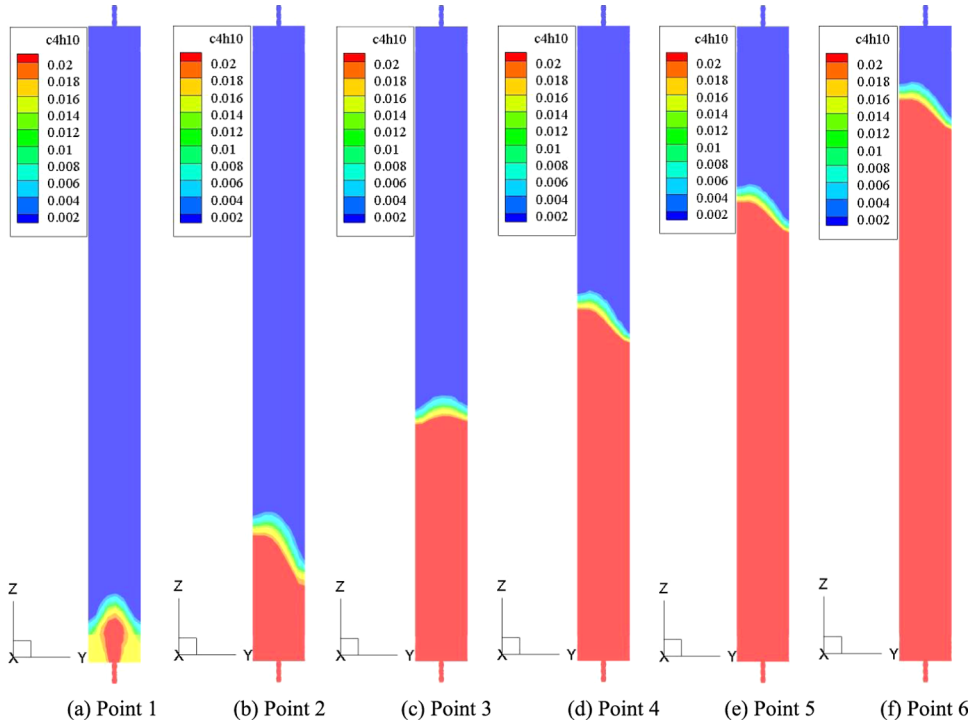

Figure 5. *n*-Butane concentration cloud images of the adsorption process.

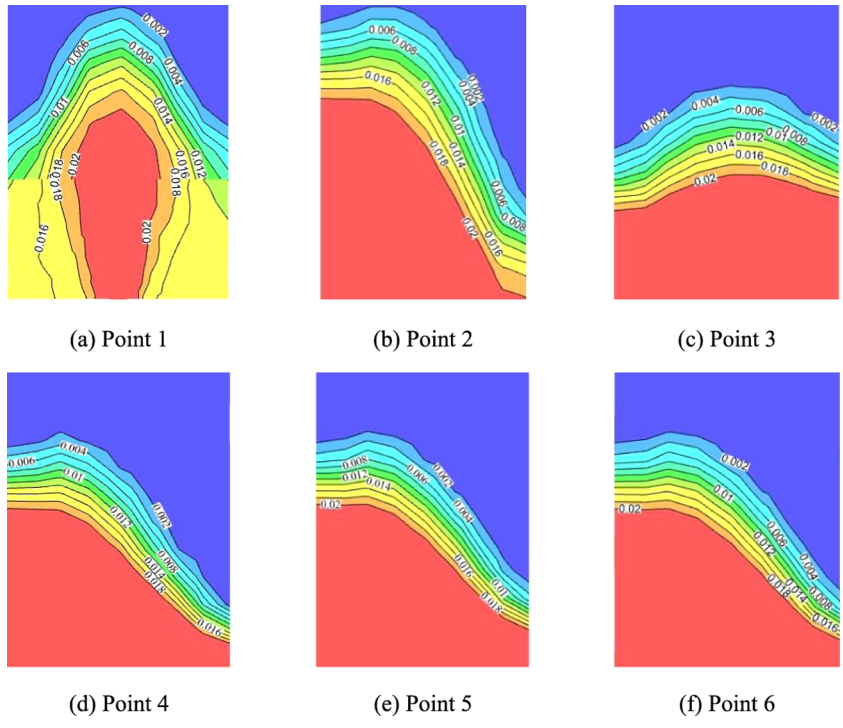

Figure 6. Isotope plot of the local *n*-butane concentration of the adsorption process.

In Figure 4, the background temperatures of point 1 and point 6 were 300.5 and 301 K, respectively. The initial temperature of the fixed bed was set as 300 K, and the temperature of the whole bed increased approximately 1 K. From Figure 4, we can see that the maximum temperatures of points 1−6 are 7.5, 6.5, 6, 8, 9, and 9.5 K respectively. The maximum temperatures of the first three monitoring points decreased gradually, and those of the latter three points increased. Because under the continuous purging of the inlet gas, the heat generated by the first half of the fixed bed is purged to the second half, and as a result, the fixed bed's background temperature is increased.

Figures 3 and 4 show that the closer to the center of the fixed bed, the higher the temperature. However, the closer to the center of the fixed bed, the more difficult it was to transfer heat to the outside.

The *n*-butane concentration cloud images of the fixed bed are shown in Figure 5, and the isotope plot of the *n*-butane concentration of adsorption is shown in Figure 6.

https://doi.org/10.1021/acsomega.0c06273
ACS Omega 2021, 6, 17162−17172

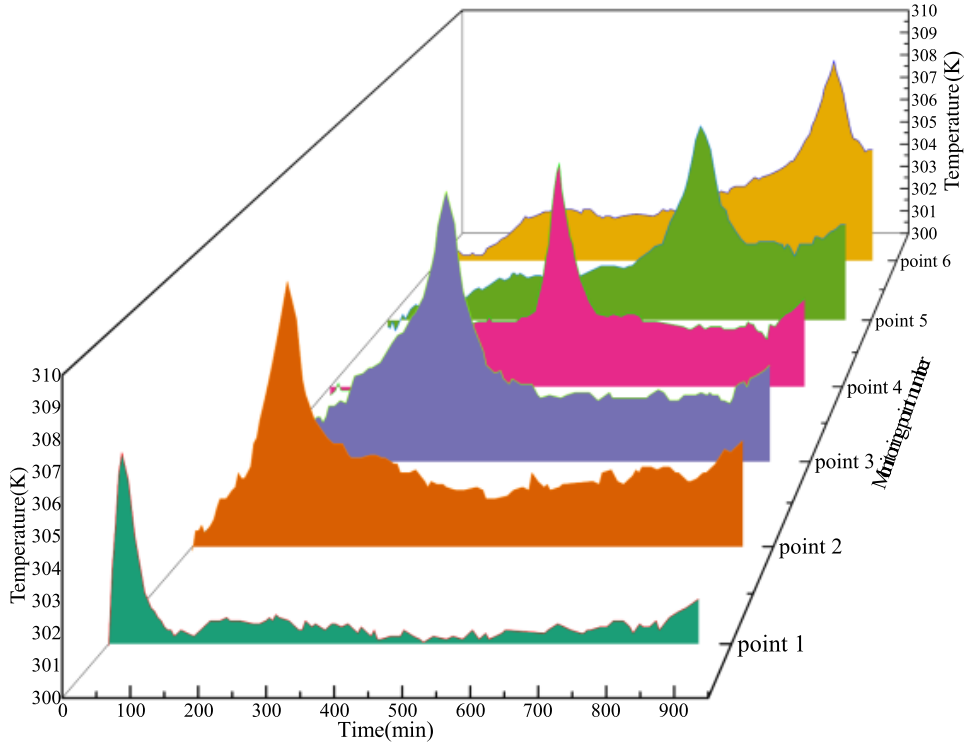

Figure 7. Experimental data of temperature at six monitoring points of the adsorption process.

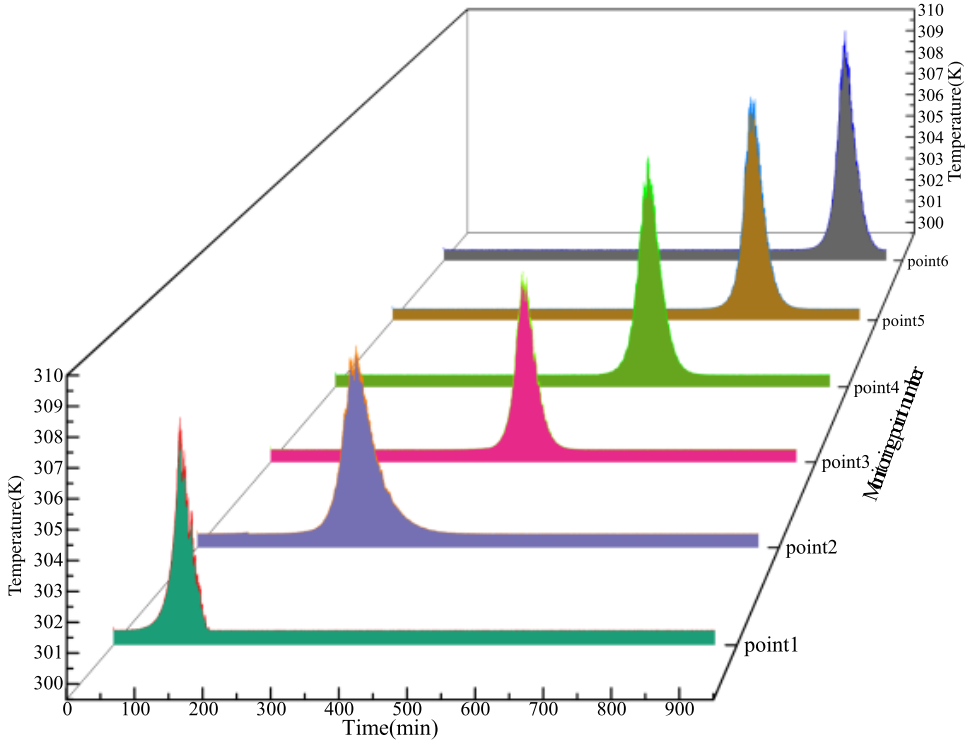

Figure 8. Simulative data of temperature at six monitoring points of the adsorption process.

The region between the saturated and nonadsorbed regions was denoted as the adsorbed belt. Figures 5 and 6 show that the adsorbed belt moves forward gradually because, under the sweeping action of the airflow, when the *n*-butane gas was adsorbed by AC, the AC gradually became saturated and the adsorbed belt moved forward. The adsorbed belt was curved, with its top at the center of the fixed bed, and the direction was consistent with the direction of the airflow. As the inlet was located in the middle of the fixed bed, the airflow entering the AC area was faster near the center, which causes the AC in the middle to become saturated earlier than that on both sides, thus forming the arc-shaped adsorbed belt.

https://doi.org/10.1021/acsomega.0c06273
ACS Omega 2021, 6, 17162−17172

Figures 3 and 5 show that the adsorbed belt is consistent with the higher temperature distribution of the fixed bed. The process of organic gas adsorption by AC was mass transfer, and the process of organic gas adsorption to release heat was heat transfer. This indicates that the AC adsorption process is simultaneous mass and heat transfer and reflects the synchronization and consistency of the fluid mass- and heat-transfer processes.

2.3.2. Data Validation and Analysis. The temperature changes of the six monitoring points of the fixed bed of AC are shown in Figure 7, and the ΔT_{max} of each monitoring point is given in Table 4. The temperature curves are parabola, and the transverse span is basically the same, which shows that the length of the mass-transfer belt is almost the same as that in the adsorption process, the temperature changes obviously along the airflow direction in the bed, the maximum temperature increase area is transmitted along the air inlet direction, and the maximum temperature increase value on the mass-transfer belt is between 7 and 10 K. The maximum temperatures at the simulated and experimental process points 1−6 are shown in Figure 7. Simulative data of temperature at six monitoring points of the adsorption process are shown in Figure 8; the trend of the simulation data is consistent with that of the experimental data, and the range of the temperature change is small. This reflects the correctness of the simulation data for the heat-transfer process of the fixed bed.

The deviation rates of the experimental and simulated temperatures at six points are shown in Table 1. The deviation rate between the simulated and experimental temperatures was between 0.162 and 1.290%, which is well below 5%, and the deviation rate between the simulated adsorption breakthrough time 895 min and the experimental adsorption breakthrough time 924 min was 3.139%. This demonstrates the accuracy of the simulation results obtained using Fluent.

Table 1. Deviation Rate between the Simulated and Experimental Temperatures

	point 1	point 2	point 3	point 4	point 5	point 6
simulated data (K)	307.5	306.5	306	308	309	309.5
experimental data (K)	307	309.2	310	309.2	308.5	309
deviation rate (%)	0.163	0.873	1.290	0.388	0.162	0.162

Figure 9 shows the changes in the concentration of *n*-butane at the six monitoring points and the outlet. The trend of the *n*-butane concentration at the seven points was consistent, reflecting the stability of the AC adsorption process. The trend was consistent by comparing outlet concentrations obtained in the experiments and simulated results, which reflects the reliability of the simulation data. The simulated breakthrough time of adsorption was approximately 895 min, and the experimental breakthrough time was approximately 924 min. The breakthrough time of the simulated process was shorter than that of the experimental process because, in the simulation process, the particle size of AC was fairly uniform and the distribution of AC was regular, which results in a higher adsorption efficiency and shorter time required to simulate adsorption saturation.

3. CONCLUSIONS

In this study, a multidimensional transient model for the adsorption process of an AC fixed bed was established, and the heat and mass transfer of the *n*-butane adsorbed in the fixed bed was simulated by Fluent. According to the experimental data and simulation results, the trends of the changes in the temperature and concentration in fixed-bed adsorption were analyzed. From the discussions in this paper, we can draw the following conclusions:

(1) The simulation results were compared with the experimental results of the absorption process. The deviation ratio between the simulated and experimental temperatures at six points ranged from 0.162 to 1.290%. The trend of the simulated outlet concentration was consistent with that of the experimental outlet concentration, and the accuracy and reliability of the simulation

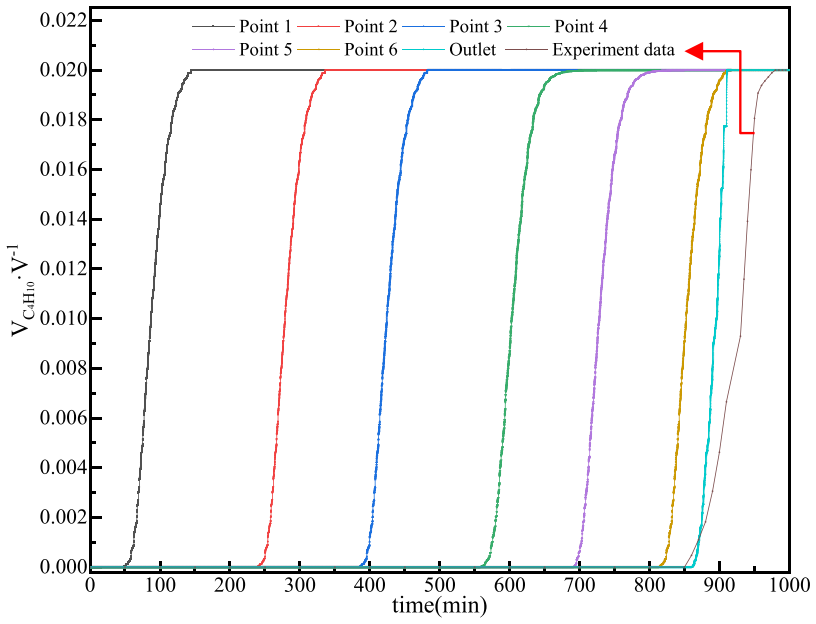

Figure 9. Comparison of the experimental and simulated concentration change curves.

https://doi.org/10.1021/acsomega.0c06273
ACS Omega 2021, 6, 17162−17172

process and results were demonstrated. The simulation results have value as a reference for industrial applications of AC adsorption.

(2) Temperature cloud images show that the temperature increase at the center of the fixed bed was larger during the whole adsorption process. *n*-Butane concentration cloud images show that the adsorbed belt was curved, and the AC at the center of the fixed bed becomes saturated more rapidly than that on both sides. In the design of the fixed bed, the heat release can be promoted by adjusting the arrangement of AC particles and the packing density in the middle of the fixed bed. The simulation results can provide a reference for the design and modification of the fixed bed.

4. EXPERIMENTAL SECTION

The AC was supplied by Mead Westvaco (MWV) Co. Ltd. (Shanghai, China). Also, its properties and parameters are shown in Table 2. Experimental pretreatment:

Table 2. AC Properties and Parameters

AC type	AC quality m_{AC} (g)	valid diameter D_p (mm)	porosity ε	density ρ_{AC} ($kg{\cdot}m^{-3}$)	specific heat capacity $c_{p_{AC}}$ ($J{\cdot}kg^{-1}{\cdot}K^{-1}$)
WV-A1500	217	0. 85	0.38	550	840

4.1. Equilibrium Adsorption Capacity Experiment. The equilibrium adsorption capacity (q_e) of AC for *n*-butane was determined by conducting flow adsorption equipment (Figure 10) at room temperature and 1.0 atm. After preheating and pretreatment, approximately 0.65 g of AC was added to a U-tube with an inside diameter of 4 mm. The total gas flow was controlled using mass flow meters to maintain a constant flow rate of 30 $mL{\cdot}min^{-1}$, and the concentration of *n*-butane in the intake gas ranged from 250 ppm (10^{-6}V/V) to 2000 ppm (10^{-6}V/V). The U-tube mass was weighed at 25 min intervals until the value became stable.

The equilibrium adsorption capacities (q_e, g_{VOCs}/g_{adsorb}) of the adsorbents were measured and calculated by eq 9

$$q_e = \frac{W_A - W_B}{W_S} \tag{9}$$

where W_A and W_B are the weights of the tube after and before adsorption, respectively, (g), and W_S is the weight of samples before adsorption (g).

4.2. Breakthrough Curve and Temperature Experiment. The breakthrough curve and temperature in the fixed bed were tested in the equipment (Figure 11), and a 450 mm long 304 stainless steel pipe with an inside diameter of 35 mm was used as the adsorption column.

After 30 min of nitrogen purging pretreatment, a stream mixture with 20 000 ppm (10^{-6}V/V) of *n*-butane/N_2 (400 $mL{\cdot}min^{-1}$) was passed through the fixed bed. The breakthrough curves were obtained by recording the concentration of *n*-butane at the outlet of the adsorption column, which was continuously monitored using a gas chromatograph (GC) equipped with a total hydrocarbon-filling column (3 × 2000 mm) and an FID detector.

Six thermocouples were used to monitor the changes in the bed temperature during adsorption. The thermocouple positions were defined with respect to the inlet ($z = 0$) and tank axis ($r = 0$). Thermocouple P_6 was located at the entrance of the tank ($z = 45$ mm, $r = 0$); P_5 at $z = 120$ mm, $r = 0$; P_4 at $z = 195$ mm, $r = 0$; P_3 at $z = 270$ mm, $r = 0$; P_2 at $z = 345$ mm, $r = 0$; and P_1 was located at the outlet of the tank ($z = 420$ mm, $r = 0$).

5. COMPUTATIONAL METHODS

5.1. Adsorption Capacity. To trace the adsorption capacity changes in the adsorption process, isotherms of *n*-butane on AC were fitted by the Langmuir model[38,39] with the following formula (eq 10).

$$\frac{C_e}{q_e} = \frac{1}{q_{max}{\cdot}b} + \frac{C_e}{q_{max}} \tag{10}$$

where q_{max} is the maximum adsorption capacity ($g{\cdot}g^{-1}$), b is the Langmuir constant ($L{\cdot}mg^{-1}$), C_e is the mass concentration after adsorption equilibrium ($mg{\cdot}L^{-1}$), and q_e is the equilibrium adsorption capacity ($g{\cdot}g^{-1}$).

The adsorption capacity of *n*-butane on AC could be fitted well by the Langmuir model, as indicated by the good relative coefficients ($R^2 = 0.9871$). According to the fitting equation in Figure 12, $q_{max} = 0.2674$ $g{\cdot}g^{-1}$ and $b = 0.00299$ $L{\cdot}mg^{-1}$. Therefore, the maximum adsorption capacity q_{max} of AC was 0.2674 $g{\cdot}g^{-1}$.

5.2. Adsorption Kinetic Parameters. *5.2.1. Yoon–Nelson Model.* The Yoon–Nelson model[40] is a relatively simple model for the adsorption of gases on AC. This model assumes that the diminution rate during adsorption for every adsorbate molecule is relative to the probability of solute breakthrough on the adsorbent. The equation for this model is described by the following formula (eq 11).

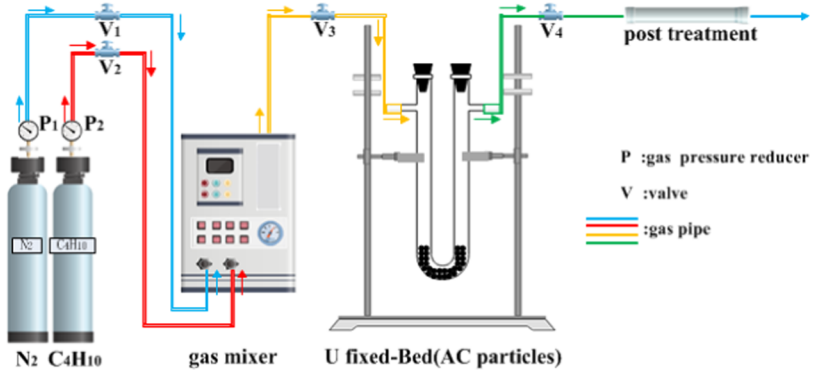

Figure 10. Schematic diagram of the VOC adsorption equipment on the U fixed bed.

https://doi.org/10.1021/acsomega.0c06273
ACS Omega 2021, 6, 17162−17172

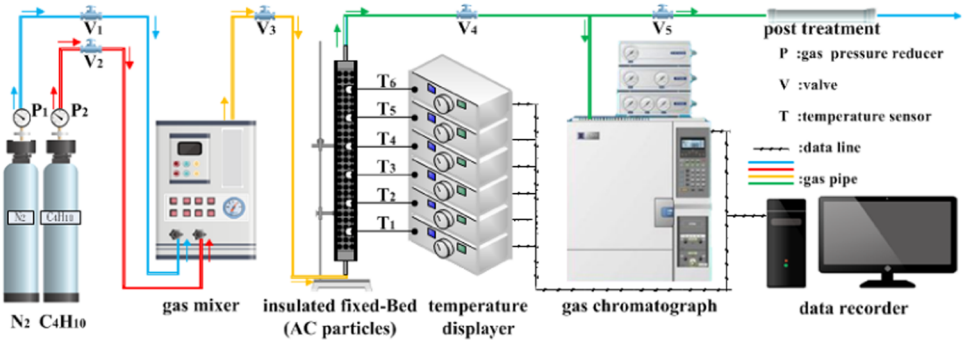

Figure 11. Schematic diagram of the VOC adsorption experiment system in the insulated fixed bed.

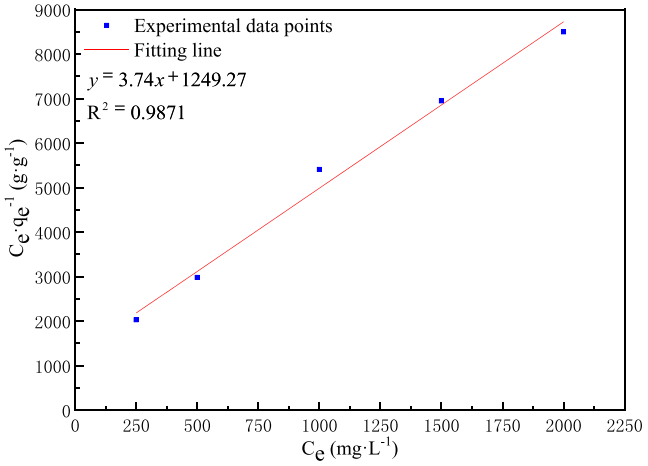

Figure 12. Fitting diagram of the adsorption capacity based on the Langmuir equation.

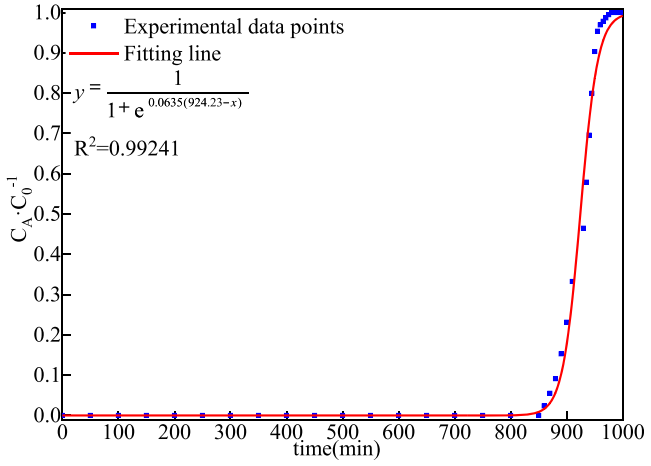

Figure 13. Breakthrough curves and mathematic models of AC samples.

$$\frac{C_A}{C_0} = \frac{1}{1 + \exp[k'(\tau_0 - t)]} \quad (11)$$

where C_A and C_0 are the outlet and inlet concentrations of the stream gas (ppm), respectively, τ_0 is the breakthrough time (time for $C_A = 0.5\ C_0$), and k' is the Yoon−Nelson constant.

The fitting results of the Yoon−Nelson model are shown in Figure 13 and Table 3. According to the adsorption breakthrough curve, the total amount of *n*-butane adsorbed by AC is 19.135 g, i.e., $n_{C_4H_{10}} = 0.328$ mol.

5.2.2. First-Order Kinetics Equation Model. The first-order kinetics equation (eq 12) was used to fit the adsorption breakthrough curve, and the results are shown in Figure 14 and Table 3.

The first-order kinetics equation[41] is described by the following formula (eq 12).

$$q = q_e - q_e e^{-k_1 t} \quad (12)$$

where t is the time (min), q_e is the equilibrium adsorption capacity (mg·g^{-1}), q_t is the adsorption capacity of *n*-butane at time t (mg·g^{-1}), and k_1 is the first-order adsorption rate constant (min^{-1}).

According to the fitting equation of the Yoon−Nelson adsorption model, the adsorption breakthrough time is 924 min. It can be seen from the correlation coefficient R^2 that the Yoon−Nelson adsorption model and first-order kinetics equation have high goodness of fit with the adsorption breakthrough curve, indicating that the adsorption process of *n*-butane on AC is physical adsorption.

Table 3. Fitting Kinetic Parameters of Adsorption of *n*-Butane by AC with Different Models

	Yoon−Nelson adsorption model			first-order dynamic equation	
temperature (K)	k' (min^{-1})	τ_0 (min)	R^2	k_1 (min^{-1})	R^2
300	0.0635	924	0.992	0.02386	0.953

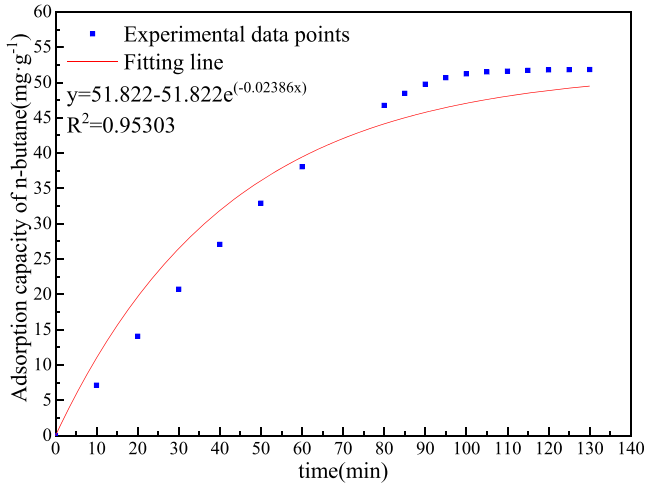

Figure 14. Fitting curve of first-order adsorption kinetics equation.

5.3. Adsorption Heat. In the adsorption process, the gas molecules move to the solid surface, the molecular movement speed is greatly reduced, and the heat is released. The adsorption

https://doi.org/10.1021/acsomega.0c06273
ACS Omega 2021, 6, 17162−17172

heat is one of the important indicators to measure the performance of the adsorbent.[42]

The maximum temperature increase values (ΔT_{max}) of the six monitoring points in the adsorption experiment are shown in Table 4.

Table 4. Maximum Temperature Increase Values of Six Monitoring Points

number	point 1	point 2	point 3	point 4	point 5	point 6
ΔT_{max} (K)	7	9.2	10	9.2	8.5	9

When the adsorption of *n*-butane by AC particles reaches the saturation state, the heat is no longer released, and the adsorbed *n*-butane molecules and free *n*-butane molecules in the AC are in a thermal dynamic equilibrium state. The distribution of *n*-butane obeys Boltzmann distribution, and the adsorption heat of two-energy-state model ε_a[43,44] formula is (eq 13)

$$\varepsilon_a = kT \ln \frac{N_1}{N_2} \tag{13}$$

where k is the Boltzman number (1.380649×10^{-23} J·K^{-1}), T is the temperature (K), N_1 is the molecular number of free *n*-butane, and N_2 is the molecular number of adsorbed *n*-butane.

The total adsorption heat Q_a is

$$Q_a = N_2 kT \ln \frac{N_1}{N_2} \tag{14}$$

Under the standard condition, 90% of the adsorbed *n*-butane is in the adsorbed state and 10% is in the free state.[43] The ambient temperature of this adsorption experiment is 300 K, and the ratio of the molecular number of adsorbed and free *n*-butane is $N_1/N_2 = 9{:}1$. According to the adsorption heat formula of two-energy-state model (eq 15),[32,33] the theoretical adsorption heat of AC adsorbing *n*-butane ($Q_{a,t}$) can be calculated

$$Q_{a,t} = -N_A \varepsilon_a = -RT \ln \frac{N_1}{N_2} = 5.48\ \text{kJ·mol}^{-1} \tag{15}$$

where N_A is the Avogadro constant (6.02×10^{23}).

The theoretical adsorption heat of *n*-butane on AC is 5.48 kJ·mol^{-1}.

The mass of *n*-butane adsorbed by AC is $n_{C_4H_{10}} = 0.328$ mol, and the maximum temperature increase is $\Delta T_{max} = 10$ K (Table 4). The actual adsorption heat of AC adsorbing *n*-butane ($Q_{a,a}$) in the experiment can be calculated

$$Q_{a,a} = \frac{c_{p_{AC}} \cdot m_{AC} \cdot \Delta T_{max}}{n_{C_4H_{10}}} = 5.56\ \text{kJ·mol}^{-1} \tag{16}$$

The deviation rate between $Q_{a,t}$ and $Q_{a,a}$ is 1.44%; the actual adsorption heat is consistent with the theoretical adsorption heat. The results show that the adsorption of *n*-butane by AC belongs to physical adsorption. The adsorption heat of n-butane on AC is $Q_{a,a} = 5.56$ kJ·mol^{-1}.

AUTHOR INFORMATION

Corresponding Author

Ling Zhu − *Department of Environmental Engineering, Beijing Institute of Petrochemical Technology, Beijing 102617, China;* orcid.org/0000-0003-3883-9509; Email: zhuling75@bipt.edu.cn

Authors

Fei Zhao − *Department of Environmental Engineering, Beijing Institute of Petrochemical Technology, Beijing 102617, China*

Zhenzhong Wang − *SINOPEC Research Institute of Safety Engineering, Qingdao, Shandong 266071, China*

Yan Hou − *Department of Environmental Engineering, Beijing Institute of Petrochemical Technology, Beijing 102617, China*

Jiaqing Chen − *Department of Environmental Engineering, Beijing Institute of Petrochemical Technology, Beijing 102617, China*

Chunyu Wang − *Department of Environmental Engineering, Beijing Institute of Petrochemical Technology, Beijing 102617, China; College of Environmental and Energy Engineering, Beijing University of Technology, Beijing 100124, China*

Danyun Xu − *Department of Environmental Engineering, Beijing Institute of Petrochemical Technology, Beijing 102617, China*

Complete contact information is available at: https://pubs.acs.org/10.1021/acsomega.0c06273

Notes

The authors declare no competing financial interest.

ACKNOWLEDGMENTS

This work was supported by grants from Beijing Municipal College's "Great Wall" Scholars Projects (CIT&TCD20190314), SINOPEC's Projects (320109), and the Award Cultivation Foundation from Beijing Institute of Petrochemical Technology (Project No. BIPTACF-003).

REFERENCES

(1) Miguet, M.; Goetz, V.; Plantard, G.; Jaeger, Y. Removal of a Chlorinated Volatile Organic Compound (Perchloroethylene) from the Aqueous Phase by Adsorption on Activated Carbon. *Ind. Eng. Chem. Res.* **2015**, *54*, 9813−9823.

(2) Zhang, Z. X.; Jiang, Z.; Shangguan, W. F. Low-temperature catalysis for VOCs removal in technology and application: A state-of-the-art review. *Catal Today.* **2016**, *264*, 270−278.

(3) He, C.; Cheng, J.; Zhang, X.; Douthwait, M.; Pattisson, S.; Hao, Z. P. Recent Advances in the Catalytic Oxidation of Volatile Organic Compounds: A Review Based on Pollutant Sorts and Sources. *Chem. Rev.* **2019**, *119*, 4471−4568.

(4) Zhang, K.; Zhang, L.; Yang, S. T. Fumaric Acid Recovery and Purification from Fermentation Broth by Activated Carbon Adsorption Followed with Desorption by Acetone. *Ind. Eng. Chem. Res.* **2014**, *53*, 12802−12808.

(5) Zhang, X. Y.; Gao, B.; Creamer, A. E.; Cao, C. C.; Li, Y. C. Adsorption of VOCs onto engineered carbon materials: A review. *J. Hazard Mater.* **2017**, *338*, 102−123.

(6) Zhang, G. X.; Feizbakhshan, M.; Zheng, S. L.; Hashishol, Z.; Sun, Z. M.; Liu, Y. Y. Effects of properties of minerals adsorbents for the adsorption and desorption of volatile organic compounds (VOC). *Appl. Clay Sci.* **2019**, *173*, 88−96.

(7) Dobre, T.; Parvulescu, O. C.; Iavorschi, G.; Stroescu, M.; Stoica, A. Volatile Organic Compounds Removal from Gas Streams by Adsorption onto Activated Carbon. *Ind. Eng. Chem. Res.* **2014**, *53*, 3622−3628.

(8) Zhang, L.; Peng, Y. X.; Zhang, J.; Chen, L.; Meng, X. J.; Xiao, F. S. Adsorptive and catalytic properties in the removal of volatile organic compounds over zeolite-based materials. *Chin. J. Catal.* **2016**, *37*, 800−809.

(9) Domingo, J. L.; Rovira, J.; Vilavert, L.; Nadal, M.; Figueras, M. J.; Schuhmacher, M. Health risks for the population living in the vicinity of an Integrated Waste Management Facility: Screening environmental pollutants. *Sci. Total Environ.* **2015**, *518*−*519*, 363−370.

(10) Huang, Y.; Ling, Z. H.; Lee, S. C.; Ho, S. S. H.; Cao, J. J.; Blake, D. R.; Cheng, Y.; Lai, S. C.; Ho, K. F.; Gao, Y.; Cui, L.; Louie, P. K. K. Characterization of volatile organic compounds at a roadside environment in Hong Kong: An investigation of influences after air pollution control strategies. *Atmos. Environ.* **2015**, *122*, 809−818.
(11) Kerminen, V. M.; Virkkula, A.; Hillamo, R.; Wexler, A. S.; Kulmala, M. Secondary organics and atmospheric cloud condensation nuclei production. *J. Geophys. Res.* **2000**, *105*, 9255−9264.
(12) Ouzzine, M.; Romero-Anaya, A. J.; Lillo-Rodenas, M. A.; Linares-Solano, A. Spherical activated carbons for the adsorption of a real multicomponent VOC mixture. *Carbon* **2019**, *148*, 214−223.
(13) Niknaddaf, S.; Atkinson, J. D.; Gholidoust, A.; Fayaz, M.; Awad, R.; Hashisho, Z.; Phillips, J. H.; Anderson, J. E.; Nichols, M. Influence of Purge Gas Flow and Heating Rates on Volatile Organic Compound Decomposition during Regeneration of an Activated Carbon Fiber Cloth. *Ind. Eng. Chem. Res.* **2020**, *59*, 3521−3530.
(14) Cho, S. H.; Lee, J.; Kim, K. H.; Jeon, Y. J.; Kwon, E. E. Carbon dioxide assisted co-pyrolysis of coal and ligno-cellulosic biomass. *Energy Convers. Manage.* **2016**, *118*, 243−252.
(15) Kamravaei, S.; Shariaty, P.; Lashaki, M. J.; Atkinson, J. D.; Hashisho, Z.; Phillips, J. H.; Anderson, J. E.; Nichols, M. Effect of Beaded Activated Carbon Fluidization on Adsorption of Volatile Organic Compounds. *Ind. Eng. Chem. Res.* **2017**, *56*, 1297−1305.
(16) Mhiri, F.; Jemni, A. Correlation Between Fluctuation and Dissipation in the Case of the Adsorption of Acetone and Ethanol by the Activated Carbon. *Environ. Prog. Sustainable Energy* **2011**, *30*, 294−302.
(17) Leporini, M.; Corvaro, F.; Marchetti, B.; Polonara, F.; Benucci, M. Experimental and numerical investigation of natural convection in tilted square cavity filled with air. *Exp. Therm. Fluid Sci.* **2018**, *99*, 572−583.
(18) Malekshah, E. H.; Salari, M. Experimental and numerical investigation of natural convection in a rectangular cuboid filled by two immiscible fluids. *Exp. Therm. Fluid Sci.* **2017**, *85*, 388−398.
(19) Li, S.; Deng, S.; Zhao, L.; Zhao, R. K.; Lin, M.; Du, Y. P.; Lian, Y. H. Mathematical modeling and numerical investigation of carbon capture by adsorption: Literature review and case study. *Appl. Energy* **2018**, *221*, 437−449.
(20) Mota, J. P. B.; Esteves, I. A. A. C.; Rostam-Abadi, M. Dynamic modelling of an adsorption storage tank using a hybrid approach combining computational fluid dynamics and process simulation. *Comput. Chem. Eng.* **2004**, *28*, 2421−2431.
(21) Bahadori, F.; Rashidi, F. CFD simulation of temperature dependent viscosity under free convection through two-layered porous media. *Contemp. Eng. Sci.* **2012**, *5*, 67−74.
(22) Hou, X. J.; Liu, X.; Liu, Z.; Yan, F. W.; Yuan, S. L.; Jin, X. In *Flow Field Simulation and Experimental Evaluation of Carbon Canister Based on Fluent*, Computational Intelligence and Software Engineering, 2010; pp 1−4.
(23) Bai, X. Y.; Isaac, K. M.; Klein, D.; Banerjee, R.; Edson, J.; Breig, W.; Oliver, L. In *Multidimensional, Time-Accurate CFD Simulation of Adsorption/Desorption in a Carbon Canister*, SAE J-Autonot Eng, 2003; pp 1−15.
(24) Lin, J. S.; Dong, M.; Ali, S.; Hipp, M. In *Vehicular Emission Performance Simulation*, SAE J-Autonot Eng, 2012; pp 1−8.
(25) Hou, Y.; Kui, Y. H.; Zhu, L.; Chen, J. Q.; Sun, D. L.; Zou, Y. The numerical simulation of activated carbon absorbing benzene. *Environ. Eng.* **2016**, *34*, 471−474.
(26) Hou, Y.; Gong, Y.; Zhu, L.; Chen, J. Q. Experimental and numerical simulation study on the process parameters of benzene adsorption on activated carbon. *Ind. Saf. Environ. Prot.* **2017**, *43*, 76−80.
(27) Tao, W. Q. *Numerical Heat Transfer*, 2nd ed; Xi'an Jiaotong University: Shaanxi, 2001.
(28) Patankar, S. V. *Numerical Heat Transfer And Fluid Flow*, 1st ed.; Taylor & Francis: London, 1978.
(29) Eckert, E. R. G.; Drake, R. M. J. *Analysis Of Heat And Mass Transfer*, 1st ed.; McGraw-Hill, 1972.
(30) Wang, H. Y.; Liu, Y. S.; Zhang, C. Z.; Yang, X.; Chen, J. W. Study on variable mass flow laws in π-shaped centripetal radial flow adsorber. *CIESC J.* **2019**, *9*, 3385−3395.
(31) van Walsem, J.; Verbruggen, S. W.; Modde, B.; Lenaerts, S.; Denys, S. CFD investigation of a multi-tube photocatalytic reactor in non-steady-state conditions. *Chem. Eng. J.* **2016**, *304*, 808−816.
(32) Zhu, X. Q.; Liu, Y. S.; Yang, X.; Liu, W. H. Study of a novel rapid vacuum pressure swing adsorption process with intermediate gas pressurization for producing oxygen. *Adsorption* **2017**, *23*, 175−184.
(33) Bai, X. Y.; Isaac, K. M.; Banerjee, R.; Klein, D.; Breig, W.; Oliver, L. In *Modeling and Simulation of n-Butane Adsorption/Desorption in a Carbon Canister*, SAE J-Automot Eng, 2004; pp 1−18.
(34) Li, G.; Xiao, P.; Zhang, J.; Webley, P. A. The Role of Water on Postcombustion CO_2 Capture by Vacuum Swing Adsorption: Bed Layering and Purge to Feed Ratio. *AIChE J.* **2014**, *60*, 673−689.
(35) Zheng, Q. R.; Birkett, G.; Do, D. D. Theoretical and experimental analysis of methane adsorption on activated carbon *Nat. Gas. Chem. Ind.* 2009.
(36) Murialdo, M.; Ahn, C. C.; Fultz, B. A Thermodynamic Investigation of Adsorbate-Adsorbate Interactions of Carbon Dioxide on Nanostructured Carbons. *AIChE J.* **2018**, *64*, 1026−1033.
(37) Jegede, O. O.; Critoph, R. E. Extraction of heat transfer parameters in active carbon-ammonia large temperature jump experiments. *Appl. Therm. Eng.* **2016**, *95*, 499−505.
(38) Kilislioglu, A.; Bilgin, B. Thermodynamic and Kinetic Investigations of Uranium Adsorption on Amberlite IR-118H Resin. *Appl. Radiat. Isot.* **2003**, *58*, 155−160.
(39) Liu, Q.; Shi, J.; Zheng, S.; Tao, M.; He, Y.; Shi, Y. Kinetics Studies of CO_2 Adsorption/Desorption on Amine-Functionalized Multiwalled Carbon Nanotubes. *Ind. Eng. Chem. Res.* **2014**, *53*, 11677−11683.
(40) Vizhemehr, A. K.; Haghighat, F.; Lee, C. S. Gas-phase filters breakthrough models at low concentration - Effect of relative humidity. *Build. Environ.* **2014**, *75*, 1−10.
(41) Martí-Rosselló, T.; Jun, L.; Leo, L. Quantitatively modelling kinetics through a visual analysis of the derivative thermogravimetric curves: Application to biomass pyrolysis. *Energy Convers. Manage.* **2018**, *172*, 296−305.
(42) Zhou, R. F.; SHI, J. H.; Liu, Q. Z.; Mou, S. J.; Jiang, C. M.; Gong, L. Molecular simulation on adsorption of methane and toluene by activated carbon. *Chin. J. Process Eng.* **2018**, *9*, 2476−2483.
(43) Liu, Z. X.; Feng, Z. C. Theoretical study on adsorption heat of methane in coal. *J. China Coal Soc.* **2012**, *4*, 647−653.
(44) Feng, Z. C.; Zhao, D.; Liu, Z. X.; Wang, Y. Q.; Gou, H. Q. Two-state energy model and experimental study of coal adsorb methane. *J. Coal Sci. Eng. (China)* **2013**, *19*, 488−492.

https://doi.org/10.1021/acsomega.0c06273
ACS Omega 2021, 6, 17162−17172